Cancer Chemother Pharmacol (2011) 68:721–731
DOI 10.1007/s00280-010-1542-3

ORIGINAL ARTICLE

Effect of radiation on the penetration of irinotecan in rat cerebrospinal fluid

Amit Khatri · M. Waleed Gaber · Richard C. Brundage · Michael D. Naimark · Suzan K. Hanna · Clinton F. Stewart · Mark N. Kirstein

Received: 6 August 2010 / Accepted: 26 November 2010 / Published online: 16 December 2010

Abstract
Purpose Anticancer agents are useful for treating brain tumors, but sub therapeutic concentrations due to decreased blood–brain barrier (BBB) penetration limit their effectiveness. This study evaluated the effect of cranial radiation on the pharmacokinetics of irinotecan in plasma and cerebrospinal fluid (CSF).
Methods Rats ($n = 48$) were treated with irinotecan (10 mg/kg), and then administered 10 or 20 Gy or sham irradiation as control after drug. The pharmacokinetics for irinotecan, SN-38, and APC were measured in plasma and CSF over 6 h. Up to 7 plasma samples per animal were collected, and one CSF sample was collected per animal (serial sacrifice design). Population pharmacokinetic analysis was performed with NONMEM, and radiation tested as a covariate for the fraction of irinotecan (f_{CSF}) entering the CSF.
Results The estimate of f_{CSF} (% and RSE) was 0.165 (73.5) for the control group and 0.265 (66.5) for radiation-treated groups, respectively ($P < 0.05$). Predictive check plots showed that the model adequately described the overall trend and variability in the observed data. The median values of bootstrap parameters were similar to the NONMEM estimates based on the original data set.
Conclusions These results indicate that cranially administered radiation can increase the penetration of anticancer agents such as irinotecan into the CSF. Studies that evaluate radiation-fractionation, radiation-time course effect relationships, blood–brain barrier and blood-tumor barrier effects for irinotecan and other anticancer agents are warranted.

Keywords Irinotecan · Radiation · Cerebrospinal fluid · Pharmacokinetics

Introduction

Standard treatment for brain tumors includes surgery, radiation therapy, and chemotherapy; however, significant improvement in the outcomes for patients with malignant gliomas remains elusive. Chemotherapy is used in the adjuvant setting for patients diagnosed with astrocytomas, anaplastic gliomas, and glioblastoma, and as salvage therapy for those with the latter two. Unfortunately, drug penetration to the brain is limited by the blood–brain barrier (BBB), resulting in sub-therapeutic concentrations [1]. Active drugs against gliomas include temozolomide, irinotecan, carmustine procarbazine, carboplatin, lomustine, and other nitrosoureas (NCCN Clinical Practice Guidelines, accessed July 7, 2010).

Irinotecan (CPT-11; 7-ethyl-10-[4-(1-piperidino)-1-piperidino] carbonyloxycamptothecin), a topoisomerase I inhibitor, is approved as part of first-line therapy for

Co-first author: M. W. Gaber.

A. Khatri · R. C. Brundage · M. N. Kirstein (✉)
Department of Experimental and Clinical Pharmacology, College of Pharmacy, University of Minnesota, 717 DelawareSt S.E.,, Minneapolis, MN, USA
e-mail: kirst002@umn.edu

M. W. Gaber
Department of Pediatrics, Baylor College of Medicine, Houston, TX, USA

M. D. Naimark · S. K. Hanna · C. F. Stewart
Department of Pharmaceutical Sciences, St. Jude Children's Research Hospital, Memphis, TN, USA

M. N. Kirstein
Masonic Cancer Center, University of Minnesota, Minneapolis, MN, USA

metastatic colorectal carcinoma. In addition, it has demonstrated activity for pancreatic, lung, cervical cancers, and lymphomas [2–5]. Irinotecan undergoes hydrolysis by carboxylesterases to form the active SN-38 molecule [6], which is subsequently inactivated by glucuronidation [7]. Irinotecan can also be metabolized by CYP3A enzymes to form the oxidative metabolites, NPC, and APC [8, 9].

In early studies, irinotecan showed modest single-agent activity against recurrent malignant gliomas (15% partial response rate and 55% stable disease) [10]. Based on activity of bevacizumab plus irinotecan against colorectal tumors, this combination has been evaluated for the treatment of recurrent gliomas. In the adult population, estimated 6-month progression-free survival is 50% and median overall survival is approximately 9 months [11]. Overall survival remains dismal, and better treatments are needed.

Radiation therapy is often used after surgical removal of gliomas; however, it is associated with acute and long-term damage to the BBB and brain parenchyma [12, 13]. Following a single radiation dose to the brain, increases in BBB and blood–CSF barrier (BCSFB) permeability, leukocyte adhesion, and astrogliosis can occur [12, 14]. Such physiologic sequelae might affect the pharmacokinetics of systemically administered drugs and influence the dynamics of drug exposure to the brain and CSF. Differences between BBB and BCSFB anatomy and physiology have been reviewed elsewhere [1, 15, 16]. The CSF is continuously produced by the choroid plexus. Therefore, drugs that enter this compartment are expected to undergo changes in concentrations over time, at least partly in relation to CSF turnover. Hence, one mechanism for determining the magnitude of the affect of radiation on drug exposure to the central nervous system is to examine the changes of drug concentrations over time in CSF and plasma. As a test of concept, we therefore tested single radiation dose effects on the pharmacokinetics of irinotecan and metabolites in plasma and CSF in an animal model. Such information could be a useful step toward understanding the possible importance of combined modality therapy for the treatment of gliomas.

Materials and methods

Animals and surgical procedure

Male Sprague–Dawley rats (Charles River Laboratories, MA), 7–8 weeks of age and weighing 200–300 g, were used for the experiments. The study was approved by the institutional animal care and use committee. Principles of animal laboratory care (NIH publication No. 85–23, revised 1985) were followed. Animals were anesthetized by intra-peritoneal injection of 50 mg/kg pentobarbital sodium. Body temperature was controlled (37 ± 1°C) with a water-circulated heating mat during the course of the experiment. One catheter was placed in the femoral artery and a second in femoral vein. Irinotecan (Pfizer, NY, NY) was administered via the femoral vein, and blood samples were collected from the femoral artery. After irinotecan administration, rats were placed into one of three treatment groups. They were irradiated with a localized single dose of 10 or 20 Gy to the whole brain delivered at a rate of 2 Gy/min using an Elekta (SL-25) linear accelerator (6 MV X-rays). A circular collimator with a diameter of 1 cm was used for irradiation. A third group served as control in which they received a sham procedure. For CSF sample collection, the head of the animal was immobilized in a sterotaxic apparatus (movable z-axis) and a single sample was collected via cistern puncture for each animal.

Drug administration and sample collection

The pharmacokinetics of irinotecan and its metabolites, SN-38 and APC, were evaluated after administration of single intravenous dose of 10 mg/kg of irinotecan. Only one CSF sample was collected per animal as per the serial-sacrifice design. The collection time of CSF sample was varied between different animals in each treatment group (control, 10, or 20 Gy radiation) to capture the time course of CSF concentrations over a period of 5 h. Blood samples (about 0.5 ml) were collected via the catheter in the femoral artery at the following scheduled time points: pre, 0.25, 0.5, 1, 1.5, 2, 3, and 5 h after i.v. irinotecan administration. Blood samples were obtained only prior to obtaining the CSF samples from each animal. Hence, the number of blood samples was different between different animals depending upon when the CSF sample was taken.

Blood samples were immediately centrifuged at $5.5\times g$ for 2 min. Plasma was separated and plasma proteins were precipitated by the addition of 200 µl of plasma to 800 µl of cold methanol (−30°C), followed by vigorous agitation with vortex mixer and centrifugation at $5.5\times g$ for 2 min. The supernatant protein-free plasma was decanted and stored at −70°C until analysis.

Determination of irinotecan and its metabolites/ pharmacokinetic analysis

Irinotecan, SN-38, and APC lactone concentrations were analyzed simultaneously by an isocratic high-performance liquid chromatography assay with fluorescence detection as previously described with modification [17]. Separation was carried out at ambient temperature on a Waters (Millipore) Nova-Pak Radial-Pak C-18, reversed phase column (100 × 5 mm I.D., 4 µm particle size). The mobile phase,

0.075 M ammonium acetate buffer (pH 6.4)-acetonitrile (78:22, v/v) containing 5 mM tetrabutylammonium phosphate (TBAP) as the ion pairing reagent, was delivered at a flow rate of 1.5 ml/min. The initial excitation and emission wavelengths were 375 and 520 nm, respectively. The lower level of quantitation was 5 ng/ml for irinotecan, SN-38, and APC. All calibrators and quality control samples were prepared in rat plasma (Hill Top Lab Animals, Inc.) for the analysis of plasma samples. For CSF samples, all calibrators and quality control samples were prepared using ultra filtrate from the rat plasma using the Millipore Centrifree® YM-30.

Pharmacokinetic modeling

The population pharmacokinetic analysis for irinotecan and its metabolites was performed by means of nonlinear mixed-effects modeling using NONMEM VI (GloboMax LLC, Hanover MD) on a personal computer (Intel® Pentium D processor). The first-order conditional estimation with interaction (FOCE-I) method and ADVAN6 subroutine were used for the analysis. Model selection between competing nested models was performed by the likelihood ratio test as well as graphical goodness-of-fit diagnostics using R (version 2.9.0). To distinguish between competing nested models, a significance level of 0.05 was used, which corresponds to a decrease in OFV of at least 3.84 for 1 degree of freedom.

A sequential model building approach was used to develop the pharmacokinetic models for plasma irinotecan; metabolites APC and SN-38; and CSF irinotecan. One- and two-compartment models were tested for each of the compounds during structural model building. Models for plasma and CSF concentration–time data were parameterized in terms of clearances (CL and Q) and volumes of distribution (V). Initially, plasma irinotecan concentrations were analyzed and pharmacokinetic parameters were obtained. In the next step, the model for APC concentrations was developed. Next, the SN-38 model was developed. In the modeling of metabolite data, an assumption was made that the volume of distribution of the metabolites is same as that of irinotecan to make the model identifiable. The individual estimates of the fraction of irinotecan converted into APC (f_{APC}) and SN-38 (f_{SN}) were constrained between 0 and 1 using the logistic function shown by Eq. (1) below

$$\mathrm{fm}_i = \frac{\theta * \exp^{\eta_i}}{1 + (\theta * \exp^{\eta_i})} \quad (1)$$

where, fm_i is the fraction of irinotecan converted to a particular metabolite in the ith individual, η_i is the random effect for the ith individual, and θ is the fixed effect parameter restricted to be greater than zero. The typical value of fm (TVfm) in the population can calculated by the expression $\theta/(1 + \theta)$. The inter-individual variability of fm was approximated as shown in Eq. (2) [18]

$$\mathrm{SD}_{\mathrm{fm}} = \mathrm{TVfm} * (1 - \mathrm{TVfm}) * \left(\omega^2_{\mathrm{fm}}\right)^{1/2} \quad (2)$$

where, $\mathrm{SD}_{\mathrm{fm}}$ is the standard deviation of fm in the population and ω^2_{fm} is the variance of the random effect, η in Eq. (1) above.

Finally, the CSF irinotecan model was developed. Due to model identifiability issues, the volume of CSF was fixed to 400 µl as estimated by others [19]. In the model development, the fraction (f_{CSF}) of total elimination clearance of irinotecan responsible for the transfer of irinotecan into the CSF compartment was estimated under the assumption that the transfer of irinotecan into CSF does not affect the concentration–time profile of irinotecan in the plasma. The individual estimates of f_{CSF} were constrained between 0 and 1 using the logistic function. Since, only one CSF irinotecan concentration was collected per animal in a serial sacrifice design, the residual unexplained variability in CSF irinotecan data was fixed to the point estimate obtained from plasma irinotecan data in order to estimate the inter-individual variability in f_{CSF}. The effect of radiation was tested on f_{CSF} to determine if radiation affects the transfer of irinotecan from plasma to CSF.

Body weight (BW) and radiation treatment were tested in the covariate model building and were included in the model if they were found statistically significant at 0.05 level. BW was modeled as a power function covariate model scaled by the median BW of 251.5 g as described by Eq. (3):

$$\mathrm{TVP} = \theta_1 * \left(\frac{\mathrm{BW}}{251.5}\right)^{\theta_2} \quad (3)$$

where, TVP is the population estimate of the parameter, θ_1 is the TVP for a rat with BW of 251.5 g, θ_2 describes the steepness of the relationship between scaled BW and TVP. The effect of radiation treatment was modeled using an indicator variable. Radiation dose was also tested as a covariate, and significance was evaluated with the likelihood ratio test.

The inter-individual variability on the PK parameters was modeled according to log-normal distribution as described by Eq. (4):

$$P_i = \mathrm{TVP} * \exp(\eta_i) \quad (4)$$

where P_i is the parameter estimate for the ith individual, TVP is the population estimate of the parameter P (for a typical individual) and η_i is a random variable, which accounts for the inter-individual difference between P_i and TVP. The values of η_i were assumed to come from a normal distribution with mean of zero and variance ω^2.

The residual unexplained variability in the concentrations was described by a proportional error model as described by Eq. (5):

$$C_{ij} = F_{ij}(1 + \varepsilon_{ij}), \quad (5)$$

where C_{ij} and F_{ij} are the observed and predicted concentrations, respectively, in ith individual at jth time point; ε_{ij} is the random residual deviation between the observed (C_{ij}) and predicted (F_{ij}) concentration. The values of ε_{ij} were assumed to be independent and come from a normal distribution with mean zero and variance σ^2.

Model validation

The PK model was evaluated by performing visual predictive checks and nonparametric bootstrap analysis. For the predictive check, 500 data sets were simulated from each model using the final model parameters. The median, 5th and 95th percentiles of the simulated concentrations were calculated for a time period between 0 and 5 h after irinotecan administration. Bootstrap analysis was done to assess the stability of the PK models and to get the precision of the parameter estimates. For the bootstrap analysis, 1,000 bootstrap runs were performed using the MIfuns R-package (Metrum Institute, CT). In this technique, each individual was randomly sampled with replacement from the original data set to form new data sets having the same number of individuals as the original data set. The final model developed from the original data set was fitted to each of the bootstrap data sets to obtain the bootstrap parameter estimates. Bootstrap runs with successful minimization were used in further analysis. The median, 2.5th, and 97.5th percentiles of the parameter estimates were computed from the successful bootstrap runs and compared to the point estimates and 95% confidence intervals from the original data set.

Results

A total of 48 rats were used in the analysis with 12 rats in the control group and 18 in each of 10 and 20 Gy radiation-treatment groups. A total of 212 plasma irinotecan, 80 plasma APC, 210 plasma SN-38, and 45 CSF irinotecan concentrations were used for the model development. The various components of the PK model from the present analysis are presented in Fig. 1.

Plasma irinotecan concentration–time data were best described by a two-compartment model with inter-individual variability on volume of central compartment (V_C) and elimination CL. High correlation was observed between the inter-individual random effects (η) on CL and V_C, so a covariance term for the interaction between CL and V_C was introduced in the model. Introduction of covariance resulted in a drop of 30.2 points in the OFV and improvement in visual predictive check. Body weight (BW) was a significant covariate for V_C. The relation between BW and $V_{C\ -\ Iri}$ was described by the following model:

$$V_{C-Iri} = 2.97 * \left(\frac{BW}{251.5}\right)$$

The exponent of normalized BW in the covariate model for $V_{C\ -\ Iri}$ was not statistically significantly different from 1 and hence fixed to 1 in model development. The parameter estimates of plasma irinotecan are presented in Table 1. The typical value of V_C was found to be 2.97 l for a rat with a BW of 251.5 g. The population estimate of elimination half-lives for irinotecan in the distribution and elimination phase was 0.66 and 2.4 h, respectively. The inter-individual variability was found to be 44 and 56.5% for V_C and elimination CL, respectively. The goodness-of-fit plots for the plasma irinotecan model are presented in Fig. 2. Residual plots do not show any specific pattern, and the observed plasma irinotecan data seem to be well predicted by the model.

A one-compartment model best described APC concentration–time data with inter-individual variability on elimination clearance of APC, CL_{APC}, and fraction of irinotecan metabolized to APC, f_{APC}. The typical value of

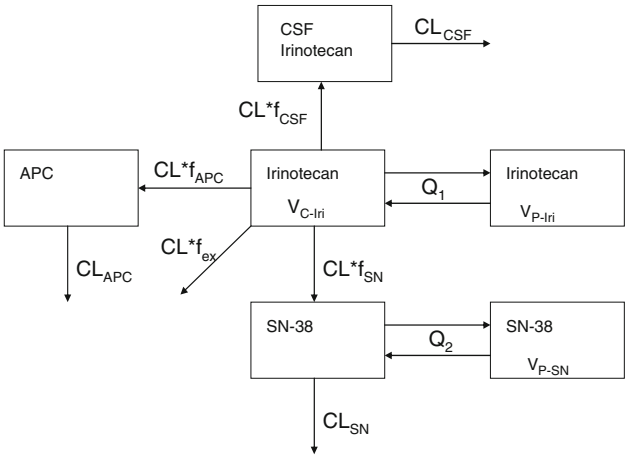

Fig. 1 Pharmacokinetic model for plasma irinotecan, APC and SN-38 and CSF irinotecan. Q_1 and Q_2 are inter-compartmental clearances. $V_{C\ -\ Iri}$ and $V_{P\ -\ Iri}$ are the volume of distribution of irinotecan for central and peripheral compartment, respectively; CL_{Iri} is the elimination clearance of irinotecan; f_{APC} is the fraction of irinotecan metabolized to APC; CL_{APC} is the elimination clearance of APC; f_{SN} is the fraction of irinotecan metabolized to SN-38; $V_{P\ -\ SN}$ is the volume of distribution of SN-38 for peripheral compartment; CL_{SN} is the elimination clearance of SN-38; f_{CSF} is the fraction of irinotecan entering into the CSF compartment; and CL_{CSF} is the elimination clearance of irinotecan from the CSF compartment; f_{ex} is the fraction of irinotecan eliminated by all other routes, and is equal to $(1 - f_{SN} + f_{APC} + f_{CSF})$

Table 1 Parameter estimates of plasma irinotecan, APC, SN-38, and CSF irinotecan model with the bootstrap results

Parameter (unit)	Estimate (RSE%)	95% CI based on NONMEM standard errors	Bootstrap estimates—Median [95% CI]
Plasma irinotecan			
V_{C-Iri} (L/251.5 g BW)	2.97 (8.15)	[2.50, 3.44]	2.85 [1.71, 3.32]
V_{P-Iri} (L)	1.3 (36)	[0.38, 2.22]	1.46 [0.75, 3.25]
Q_1 (L/H)	0.68 (37)	[0.18, 1.17]	0.80 [0.48, 3.66]
CL_{Iri} (L/H)	1.75 (9.14)	[1.43, 2.06]	1.73 [1.46, 1.99]
IIV − V_C	44.0 (29.4)	[28.6, 55.3]	44.7 [40.0, 73.5]
IIV − CL_{Iri}	56.5 (30.7)	[35.6, 71.5]	56.5 [38.7, 74.8]
Covariance (V_{C-Iri} − CL_{Iri})	0.204 (32.9)	[0.07, 0.33]	0.21 [0.11, 0.35]
RUV	25.2 (15.5)	[21.0, 28.7]	24.9 [21.7, 27.8]
APC			
f_{APC} (%)	4.5 (23.0)	[2.54, 6.67]	4.56 [3.15, 6.64]
CL_{APC} (L/H)	5.76 (18.8)	[3.64, 7.87]	5.79 [4.22, 8.15]
IIV − f_{APC}	64.1 (51.8)	[0.0, 90.45]	61.1 [26.9, 84.3]
IIV – CL	45.8 (45.7)	[14.7, 62.8]	44.7 [20.0, 63.2]
RUV	44.2 (23.3)	[32.8, 53.8]	44.7 [36.0, 53.8]
SN-38			
f_{SN} (%)	36.6 (33.9)	[16.2, 49.0]	36.0 [21.0, 54.0]
V_{P-SN} (L)	157 (24.3)	[81.9, 232.1]	151.6 [82.1, 254.9]
Q_2 (L/h)	50.2 (20.3)	[30.2, 70.2]	50.4 [26.1, 71.6]
CL_{SN} (L/H)	27.1 (32.1)	[10.0, 44.1]	25.9 [13.1, 43.4]
IIV – fm	51.5 (36.5)	[27.5, 67.4]	50.0 [27.9, 67.4]
IIV − Q_2	60.2 (58.8)	[0.0, 88.2]	61.6 [37.4, 96.9]
IIV − CL_{SN}	70.5 (49.1)	[13.7, 98.7]	72.8 [41.2, 97.9]
RUV	35.7 (12.9)	[30.8, 40.0]	35.2 [31.6, 38.9]
CSF irinotecan			
f_{CSF} (%) in control group	0.165 (73.5)	[−0.07, 0.403]	0.165 [0.013, 0.652]
f_{CSF} (%) in radiation group	0.265 (66.5)	[−0.08, 0.609]	0.261 [0.021, 0.969]
CL_{CSF} (L/h)	0.0456 (69.0)	[−0.016, 0.107]	0.044 [0.004, 0.178]
IIV − f_{CSF}	50.8 (33.4)	[29.8, 65.5]	49.9 [34.5, 63.1]

RSE relative standard error, *CI* confidence interval, *IIV* inter-individual variability, expressed as CV%, *RUV* residual explained variability, expressed as CV%

f_{APC} was estimated to be 4.5% under the assumption that the volume of distribution of APC is same as that of the central compartment of irinotecan. The population estimate of the APC elimination half-life was 0.35 h. The inter-individual variability on f_{APC} and CL_{APC} was estimated to be 64.1 and 45.8%, respectively. The goodness-of-fit plots for the plasma APC model are presented in Fig. 3. Residual plots do not show any specific pattern, and the observed plasma APC data seem to be well predicted by the model.

SN-38 concentration–time data were best described by a two-compartment model with inter-individual variability on elimination clearance of SN-38, CL_{SN}, inter-compartmental clearance, Q_2 and fraction of irinotecan metabolized to SN-38, f_{SN}. The population estimate of SN-38 terminal elimination half-life was 6.2 h, which is consistent with the previously reported values of about 4–7 h in rats [34, 38]. The inter-individual variability on CL_{SN}, Q_2 and f_{SN} was estimated to be 70.5, 60.2, and 51.5%, respectively. The goodness-of-fit plots for the plasma SN-38 model are presented in Fig. 4. Residual plots do not show any specific pattern, and the observed plasma SN-38 data seem to be well predicted by the model.

CSF irinotecan concentration–time data were best described by a one-compartment model with inter-individual variability on f_{CSF}, the fraction of total elimination clearance of irinotecan responsible for the transfer of irinotecan into CSF. The effect of radiation was tested on f_{CSF}. The estimate of f_{CSF} was 0.00165 and 0.00265 in control and radiation-treated groups, respectively; hence, f_{CSF} was 60% higher in radiation-treated groups when compared to the control group (P value < 0.05). A statistically significant difference in f_{CSF} was not observed between 10 and 20 Gy groups ($P = 0.34$);

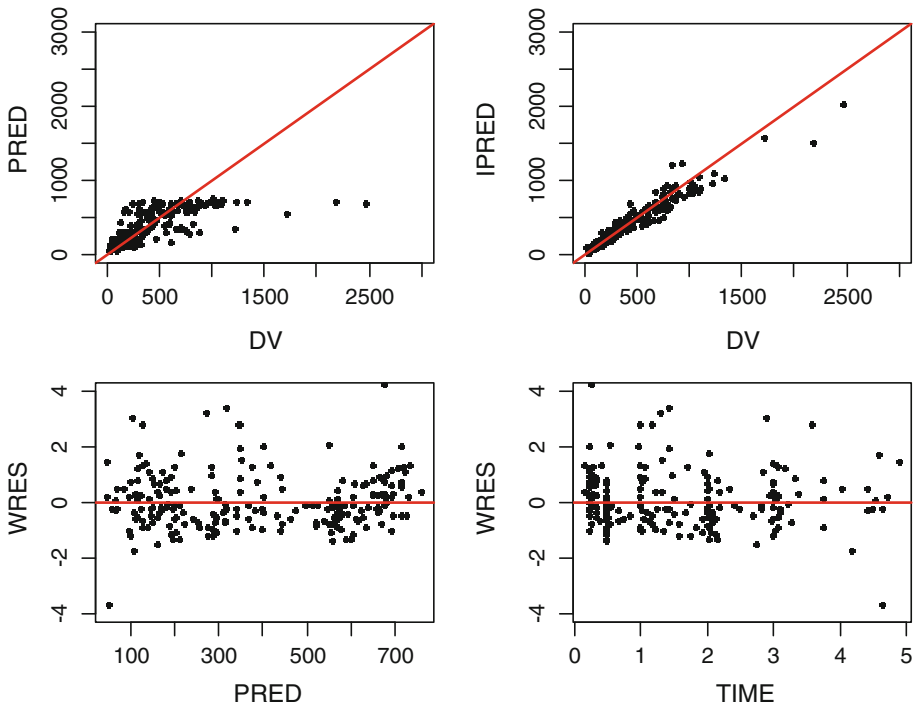

Fig. 2 Goodness-of-fit plots of plasma irinotecan model. *DV* observed concentrations, *PRED* population-predicted concentrations, and *IPRED* individual-predicted concentrations of irinotecan. *WRES* weighted residuals under the model

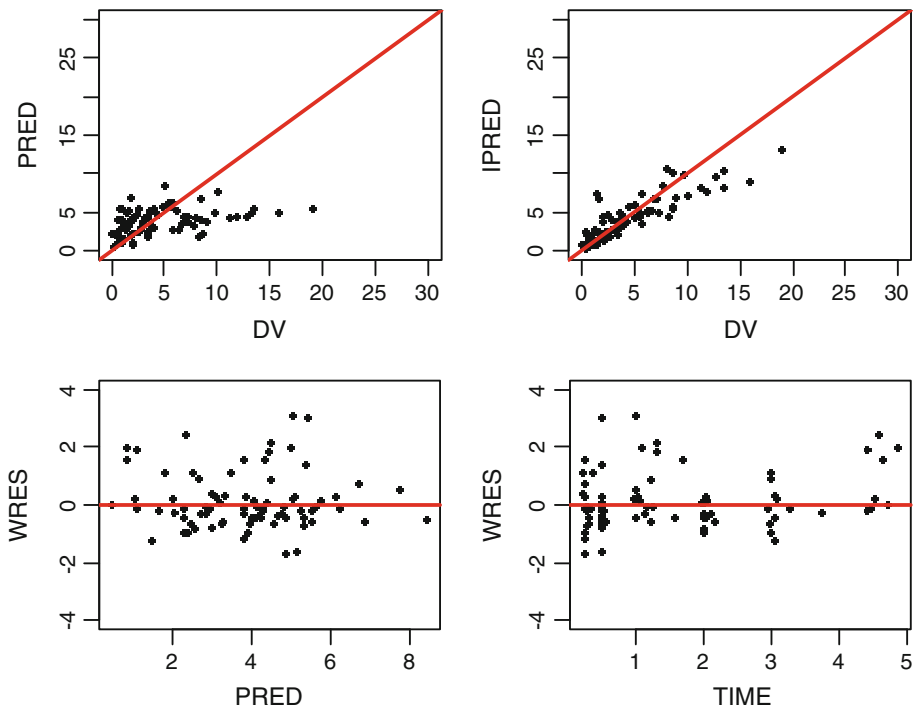

Fig. 3 Goodness-of-fit plots of plasma APC model. *DV* observed concentrations, *PRED* population-predicted concentrations, and *IPRED* individual-predicted concentrations of APC. *WRES* weighted residuals under the model

hence, the comparison was done between radiation-treated group and the control group. The inter-individual variability on f_{CSF} was estimated to be 50.8%. The goodness-of-fit plots for the CSF irinotecan model are presented in Fig. 5. Residual plots do not show any specific pattern, and the observed CSF irinotecan data seem to be well predicted by the model.

Model validation

The predictive check plots of irinotecan and metabolites, SN-38, and APC, are depicted in Fig. 6. The predictive check plots show that the model has adequately described the overall trend and variability in the observed data and do not indicate model misspecification. No systematic

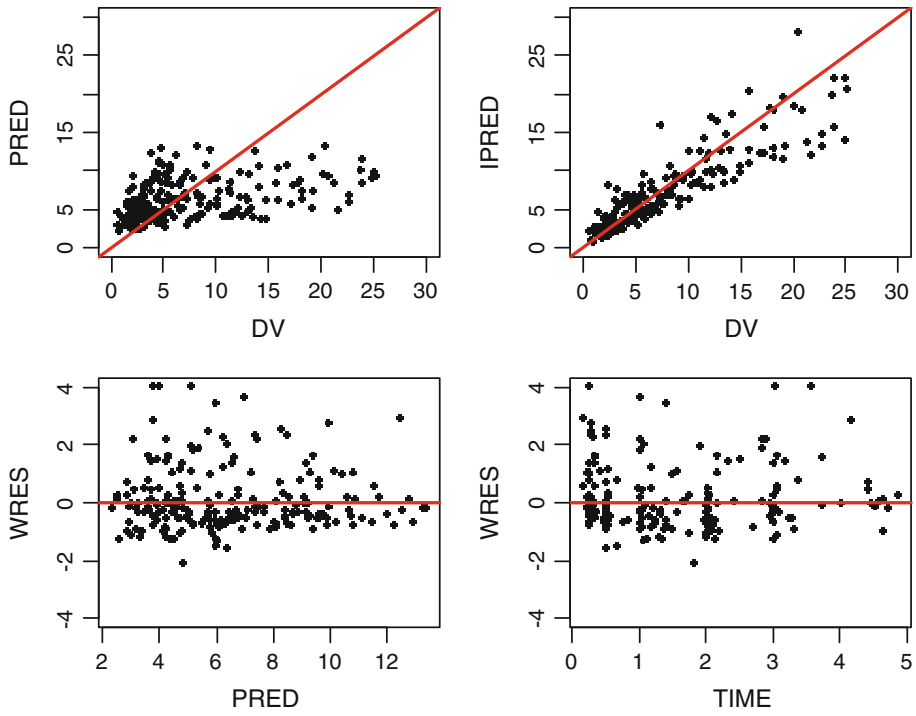

Fig. 4 Goodness-of-fit plots of plasma SN-38 model. *DV* observed concentrations, *PRED* population-predicted concentrations, and *IPRED* individual-predicted concentrations of SN-38. *WRES* weighted residuals under the model

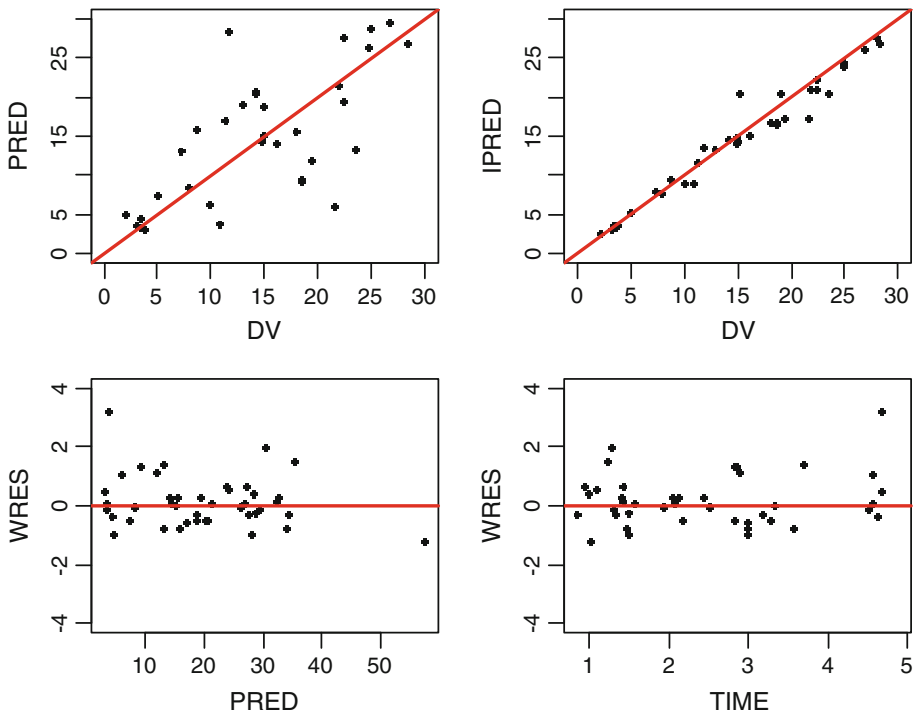

Fig. 5 Goodness-of-fit plots of CSF irinotecan model. *DV* observed concentrations, *PRED* population-predicted concentrations, and *IPRED* individual-predicted concentrations of irinotecan in CSF. *WRES* weighted residuals under the model

deviation was observed between the observed and simulated data.

In the bootstrap analysis, 927, 938, 796, and 887 runs of plasma irinotecan, APC, SN-38, and CSF irinotecan, respectively, were minimized successfully. The medians of bootstrap parameter estimates were similar to the NONMEM estimates based on original data set. Some of the parameter estimates based on original data set had relative standard error (RSE) greater than 50%, consequently their asymptotic confidence intervals include zero; however, none of the bootstrap confidence intervals include zero (Table 1). Overall, the bootstrap confidence intervals for the rest of the parameters are similar to the asymptotic confidence intervals based on NONMEM estimates.

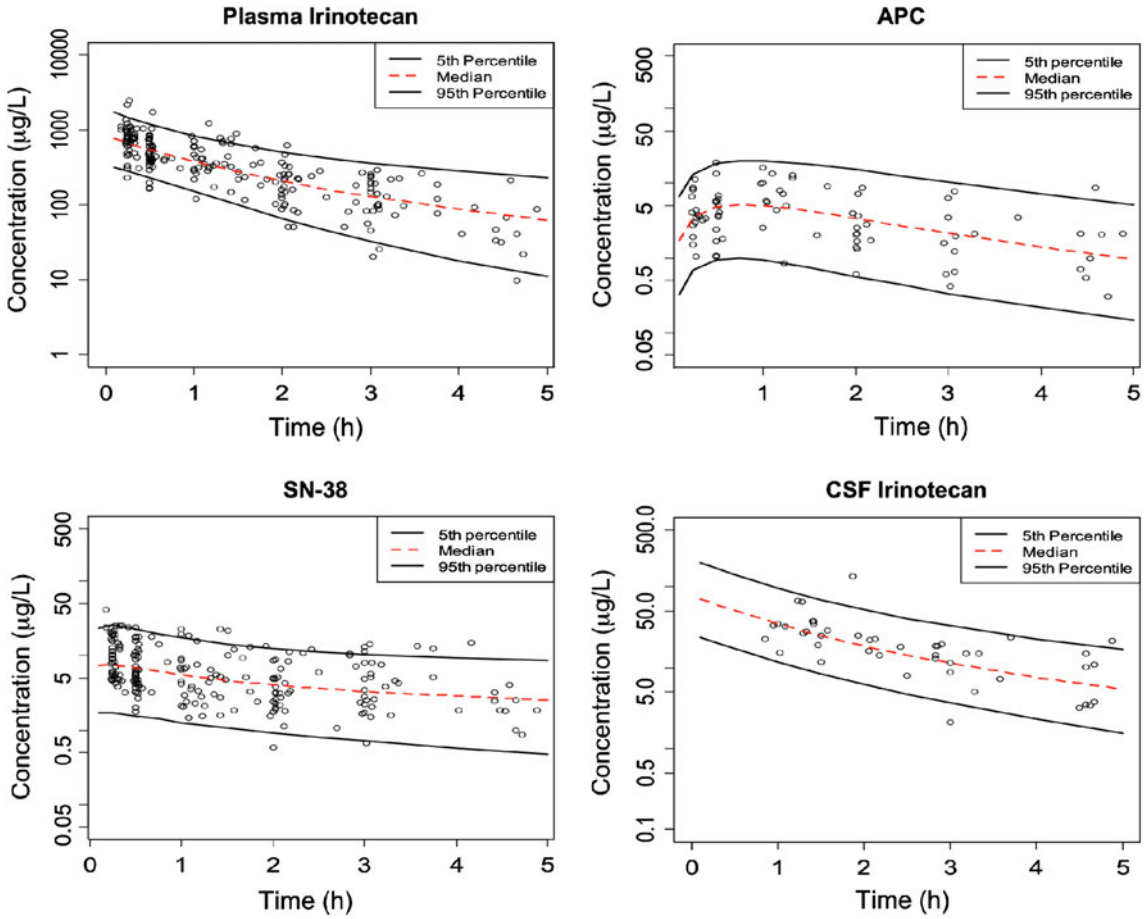

Fig. 6 Visual predictive check plots of plasma irinotecan, APC, *SN-38* and *CSF* irinotecan models. *Open circles* are observed concentrations

Discussion

Drug concentrations are easier to measure in CSF than in brain tissue in both clinical and preclinical settings; hence, CSF is a commonly used measuring site for drugs that act in the central nervous system. CSF drug concentrations may be directly relevant if the drug target sites in brain are in close contact with the ventricles, otherwise they will not necessarily provide useful information [20]. As mentioned previously, cranial radiation has been found to increase both BBB and BCSFB permeability. Hence, based on our results, we could expect that the concentration of irinotecan could also increase at the brain sites more distant from ventricles due to increase in BBB permeability; however, it would require further testing.

The CSF fills the complex interconnected ventricular cavities within the brain, the ventricles, and subarachnoid space (SAS) around the brain. This fluid is produced mainly by the choroid plexuses of the lateral and third ventricles, percolates downward into the fourth ventricle, to the roof of which is attached more choroidal tissue and then egresses into the cisterns at the brain's base. Thereafter, the CSF is convected posteriorly and downward around the spinal cord, the subarachnoid space, as well as upward over the cerebral hemispheres. Finally, CSF passes from the subarachnoid space into venous blood. Solutes, including drugs, enter into the ventricular CSF through epithelial cells of the choroid tissue by transcellular and paracellular processes and leave CSF passively at the rate of CSF turnover [21, 22].

The estimate of f_{CSF} in the CSF irinotecan model can be interpreted in terms of percentage of the administered dose of irinotecan entering into CSF, which was 0.165 and 0.265% in control and radiation-treated groups, respectively. These values depend on the value of CSF volume; however, the effect of radiation does not depend on volume. Since we fixed the value of CSF volume (400 µl), it would not affect the inference regarding the effect of radiation on f_{CSF}. Qin and colleagues reported up to threefold increase in the permeability of methotrexate in CSF after administration of 20–40 Gy dose of cranial radiation as a daily fraction of 2 Gy with five fractions per week in patients with brain tumors [23]. Increase in BBB permeability has been shown to occur as early as 2 h after

cranial irradiation with maximum increase occurring 24 h after irradiation with 20 Gy dose in rats [14]. However, information on the time-course of radiation-induced changes in BCSFB permeability is lacking. The extent of increase in BCSFB permeability could depend upon the time after irradiation and also on the dosing schedule of radiation (e.g., fractionation), which could explain the modest increase in BCSFB permeation in our study compared to up to threefold increase reported by Qin [23]. We did not observe a statistically significant difference in f_{CSF} between 10 and 20 Gy radiation groups, which could be either due to timing of maximum permeability of the BCSFB within the duration of the experiment or the BCSFB permeability reached its maximum value at or below 10 Gy dose of radiation. Irinotecan is also a known radiation sensitizer [24, 25]. Therefore, there may be enhanced antitumor effects when radiation is administered immediately after irinotecan. Others have shown that both irinotecan and SN-38 are substrates for the P-glycoprotein and MRP1 drug transporters [26, 27]. In addition, SN-38 has also been shown to be a substrate for the BCRP and OATP class of drug transporters [28, 29]. P-glycoprotein OAT3, MRP1, and MRP4 expression has been found in the choroid plexus at the BCSFB in rats as well as humans. P-glycoprotein and OAT3 are expressed in the proximity of the apical membrane of the choroid plexus, resulting in the transport of substrates into and out of the CSF, respectively. On the other hand, MRP1 and MRP4 are expressed on the basolateral side of the endothelium, resulting in the transport of substrates into the blood from the CSF [16, 30]. The presence of these transporters could also result in alteration in the exposure of irinotecan and SN-38 in brain.

Irinotecan undergoes hydrolysis by carboxylesterases (CESs) to form the active metabolite SN-38, which is highly protein-bound in plasma. Under the conditions that we tested, SN-38 concentrations in CSF remained below the limit of quantitation of our assay regardless of radiation-treatment group. High plasma protein binding could limit direct penetration of the SN-38 molecule. Two major human CESs, hCE-1 and hCE-2, have been identified in human tissues. hCE-1 is highly expressed in liver, lung epithelia, heart, and testis. hCE-2 is present in the small intestine, colon, kidney, liver, heart, brain, and testis [31]. A brain-specific CES, hCE-3, has also been identified in the brain capillary endothelial cells [32]. It is not clear that CNS enzyme activity would be sufficient to produce higher SN-38 concentrations subsequent to higher irinotecan penetration.

In the present study, an intravenous dose of 10 mg/kg of irinotecan was used, which results in maximum plasma irinotecan lactone concentrations similar to that observed in patients with cancer at clinically used doses of irinotecan [33]. Irinotecan concentration–time profiles were best described by a 2-compartment model. Body weight was found to be a significant covariate for the volume of distribution of irinotecan in the central compartment, while elimination clearance of irinotecan was found to be independent of body weight. The estimates of elimination clearance and volume of distribution of irinotecan are similar to the previously reported values in rodents [34–36]. APC concentration–time profile was best described by a one-compartment model, which is consistent with the previous reports in humans [37]. SN-38 concentration–time profile was described by a two-compartment model, which is consistent with the previous reports in rodents as well as humans [36, 37]. In general, the population fit data were not as good as the individually predicted fits. The model tended to underestimate the high concentrations, and this could be due to the high variability in plasma concentrations observed at the first time point. The results were similar, regardless of the initial estimate values tested; therefore, local minima effects on volume estimates were unlikely.

In summary, a population pharmacokinetic model was developed for irinotecan and its metabolites SN-38 and APC in rats. The final population pharmacokinetic model was judged adequate by visual predictive check and bootstrap analysis. The fraction of the administered dose of irinotecan entering into CSF was found to be about 60% higher after cranial radiation treatment when compared to the control group. Other drugs are expected to behave differently (pharmacokinetics) than irinotecan to radiation-induced perturbation of the CNS. Even though SN-38 was not detected in CSF, our studies reveal that irinotecan could be useful as a compound to evaluate the next relevant set of investigations such as radiation fractionation-effects on drug penetration (on BCSFB), radiation-time course effect relationships, BBB and blood tumor barrier effects.

Conflict of interest None.

References

1. Cecchelli R, Berezowski V, Lundquist S, Culot M, Renftel M, Dehouck MP, Fenart L (2007) Modelling of the blood-brain barrier in drug discovery and development. Nat Rev Drug Discov 6(8):650–661
2. Pizzolato JF, Saltz LB (2003) Irinotecan (Campto) in the treatment of pancreatic cancer. Expert Rev Anticancer Ther 3(5):587–593
3. Kudoh S, Fujiwara Y, Takada Y, Yamamoto H, Kinoshita A, Ariyoshi Y, Furuse K, Fukuoka M (1998) Phase II study of irinotecan combined with cisplatin in patients with previously untreated small-cell lung cancer. West Japan Lung Cancer Group. J Clin Oncol 16(3):1068–1074
4. Verschraegen CF, Levy T, Kudelka AP, Llerena E, Ende K, Freedman RS, Edwards CL, Hord M, Steger M, Kaplan AL, Kieback D, Fishman A, Kavanagh JJ (1997) Phase II study of

irinotecan in prior chemotherapy-treated squamous cell carcinoma of the cervix. J Clin Oncol 15(2):625–631
5. Ohno R, Okada K, Masaoka T, Kuramoto A, Arima T, Yoshida Y, Ariyoshi H, Ichimaru M, Sakai Y, Oguro M et al (1990) An early phase II study of CPT-11: a new derivative of camptothecin, for the treatment of leukemia and lymphoma. J Clin Oncol 8(11):1907–1912
6. Satoh T, Hosokawa M, Atsumi R, Suzuki W, Hakusui H, Nagai E (1994) Metabolic activation of CPT-11, 7-ethyl-10-[4-(1-piperidino)-1- piperidino]carbonyloxycamptothecin, a novel antitumor agent, by carboxylesterase. Biol Pharm Bull 17(5):662–664
7. Rivory LP, Robert J (1995) Identification and kinetics of a beta-glucuronide metabolite of SN-38 in human plasma after administration of the camptothecin derivative irinotecan. Cancer Chemother Pharmacol 36(2):176–179
8. Haaz MC, Rivory L, Riche C, Vernillet L, Robert J (1998) Metabolism of irinotecan (CPT-11) by human hepatic microsomes: participation of cytochrome P-450 3A and drug interactions. Cancer Res 58(3):468–472
9. Rivory LP, Riou JF, Haaz MC, Sable S, Vuilhorgne M, Commercon A, Pond SM, Robert J (1996) Identification and properties of a major plasma metabolite of irinotecan (CPT-11) isolated from the plasma of patients. Cancer Res 56(16):3689–3694
10. Friedman HS, Petros WP, Friedman AH, Schaaf LJ, Kerby T, Lawyer J, Parry M, Houghton PJ, Lovell S, Rasheed K, Cloughsey T, Stewart ES, Colvin OM, Provenzale JM, McLendon RE, Bigner DD, Cokgor I, Haglund M, Rich J, Ashley D, Malczyn J, Elfring GL, Miller LL (1999) Irinotecan therapy in adults with recurrent or progressive malignant glioma. J Clin Oncol 17(5):1516–1525
11. Friedman HS, Prados MD, Wen PY, Mikkelsen T, Schiff D, Abrey LE, Yung WK, Paleologos N, Nicholas MK, Jensen R, Vredenburgh J, Huang J, Zheng M, Cloughesy T (2009) Bevacizumab alone and in combination with irinotecan in recurrent glioblastoma. J Clin Oncol 27(28):4733–4740
12. Wilson CM, Gaber MW, Sabek OM, Zawaski JA, Merchant TE (2009) Radiation-induced astrogliosis and blood-brain barrier damage can be abrogated using anti-TNF treatment. Int J Radiat Oncol Biol Phys 74(3):934–941
13. FitzGerald TJ, Aronowitz J, Giulia Cicchetti M, Fisher G, Kadish S, Lo YC, Mayo C, McCauley S, Meyer J, Pieters R, Sherman A (2006) The effect of radiation therapy on normal tissue function. Hematol Oncol Clin North Am 20(1):141–163
14. Yuan H, Gaber MW, McColgan T, Naimark MD, Kiani MF, Merchant TE (2003) Radiation-induced permeability, leukocyte adhesion in the rat blood-brain barrier: modulation with anti-ICAM-1 antibodies. Brain Res 969(1–2):59–69
15. Spector R (2010) Nature and consequences of mammalian brain and CSF efflux transporters: four decades of progress. J Neurochem 112(1):13–23
16. Deeken JF, Loscher W (2007) The blood-brain barrier, cancer: transporters, treatment, and Trojan horses. Clin Cancer Res 13(6):1663–1674
17. Furman WL, Stewart CF, Poquette CA, Pratt CB, Santana VM, Zamboni WC, Bowman LC, Ma MK, Hoffer FA, Meyer WH, Pappo AS, Walter AW, Houghton PJ (1999) Direct translation of a protracted irinotecan schedule from a xenograft model to a phase I trial in children. J Clin Oncol 17(6):1815–1824
18. Bouzom F, Laveille C, Merdjan H, Jochemsen R (2000) Use of nonlinear mixed effect modeling for the meta-analysis of preclinical pharmacokinetic data: application to S 20342 in the rat. J Pharm Sci 89(5):603–613
19. van den Berg MP, Romeijn SG, Verhoef JC, Merkus FW (2002) Serial cerebrospinal fluid sampling in a rat model to study drug uptake from the nasal cavity. J Neurosci Methods 116(1): 99–107
20. de Lange EC, Danhof M (2002) Considerations in the use of cerebrospinal fluid pharmacokinetics to predict brain target concentrations in the clinical setting: implications of the barriers between blood and brain. Clin Pharmacokinet 41(10):691–703
21. Johanson CE, Duncan JA, Stopa EG, Baird A (2005) Enhanced prospects for drug delivery and brain targeting by the choroid plexus-CSF route. Pharm Res 22(7):1011–1037
22. Redzic ZB, Segal MB (2004) The structure of the choroid plexus and the physiology of the choroid plexus epithelium. Adv Drug Deliv Rev 56(12):1695–1716
23. Qin D, Ma J, Xiao J, Tang Z (1997) Effect of brain irradiation on blood-CSF barrier permeability of chemotherapeutic agents. Am J Clin Oncol 20(3):263–265
24. de la Fouchardiere C, Negrier S, Labrosse H, Martel Lafay I, Desseigne F, Meeus P, Tavan D, Petit-Laurent F, Rivoire M, Perol D, Carrie C (2010) Phase I study of daily irinotecan as a radiation sensitizer for locally advanced pancreatic cancer. Int J Radiat Oncol Biol Phys 77(2):409–413
25. Rich TA, Kirichenko AV (2001) Camptothecin schedule and timing of administration with irradiation. *Oncology* (*Williston Park*) 15(3 Suppl 5):37–41
26. Mathijssen RH, Marsh S, Karlsson MO, Xie R, Baker SD, Verweij J, Sparreboom A, McLeod HL (2003) Irinotecan pathway genotype analysis to predict pharmacokinetics. Clin Cancer Res 9(9):3246–3253
27. Luo FR, Paranjpe PV, Guo A, Rubin E, Sinko P (2002) Intestinal transport of irinotecan in Caco-2 cells and MDCK II cells overexpressing efflux transporters Pgp, cMOAT, and MRP1. Drug Metab Dispos 30(7):763–770
28. Han JY, Lim HS, Shin ES, Yoo YK, Park YH, Lee JE, Kim HT, Lee JS (2008) Influence of the organic anion-transporting polypeptide 1B1 (OATP1B1) polymorphisms on irinotecan-pharmacokinetics and clinical outcome of patients with advanced non-small cell lung cancer. Lung Cancer 59(1):69–75
29. Zhou Q, Sparreboom A, Tan EH, Cheung YB, Lee A, Poon D, Lee EJ, Chowbay B (2005) Pharmacogenetic profiling across the irinotecan pathway in Asian patients with cancer. Br J Clin Pharmacol 59(4):415–424
30. Urquhart BL, Kim RB (2009) Blood-brain barrier transporters and response to CNS-active drugs. Eur J Clin Pharmacol 65(11): 1063–1070
31. Imai T (2006) Human carboxylesterase isozymes: catalytic properties and rational drug design. Drug Metab Pharmacokinet 21(3):173–185
32. Mori M, Hosokawa M, Ogasawara Y, Tsukada E, Chiba K (1999) cDNA cloning, characterization and stable expression of novel human brain carboxylesterase. FEBS Lett 458(1):17–22
33. Xie R, Mathijssen RH, Sparreboom A, Verweij J, Karlsson MO (2002) Clinical pharmacokinetics of irinotecan, its metabolites: a population analysis. J Clin Oncol 20(15):3293–3301
34. Hu Z, Yang X, Ho PC, Chan E, Chan SY, Xu C, Li X, Zhu YZ, Duan W, Chen X, Huang M, Yang H, Zhou S (2005) St. John's Wort modulates the toxicities and pharmacokinetics of CPT-11 (irinotecan) in rats. Pharm Res 22(6):902–914
35. Stewart CF, Zamboni WC, Crom WR, Houghton PJ (1997) Disposition of irinotecan and SN-38 following oral and intravenous irinotecan dosing in mice. Cancer Chemother Pharmacol 40(3):259–265
36. Zamboni WC, Houghton PJ, Thompson J, Cheshire PJ, Hanna SK, Richmond LB, Lou X, Stewart CF (1998) Altered irinotecan and SN-38 disposition after intravenous and oral administration of irinotecan in mice bearing human neuroblastoma xenografts. Clin Cancer Res 4(2):455–462
37. Venook AP, Enders Klein C, Fleming G, Hollis D, Leichman CG, Hohl R, Byrd J, Budman D, Villalona M, Marshall J, Rosner GL, Ramirez J, Kastrissios H, Ratain MJ (2003) A phase I,

pharmacokinetic study of irinotecan in patients with hepatic or renal dysfunction or with prior pelvic radiation: CALGB 9863. Ann Oncol 14(12):1783–1790

38. Yang XX, Hu ZP, Chan SY, Duan W, Ho PC, Boelsterli UA, Ng KY, Chan E, Bian JS, Chen YZ, Huang M, Zhou SF (2006) Pharmacokinetic mechanisms for reduced toxicities of irinotecan by co-administered thalidomide. Curr Drug Metab 7(4): 431–455